Graphene at fluidic interfaces

Belyaeva, L.A.

Cover Page

Universiteit Leiden

The handle http://hdl.handle.net/1887/79822 holds various files of this Leiden University dissertation.

Author: Belyaeva, L.A.
Title: Graphene at fluidic interfaces
Issue Date: 2019-10-23

CHAPTER 3

Liquids relax and unify strain in graphene

Solid substrates often induce non-uniform strain and doping in graphene monolayer therefore altering the intrinsic properties of graphene, reducing its charge carrier mobilities and, consequently, the overall electrical performance. Here confocal Raman spectroscopy is exploited to study graphene directly free-floating on the surface of water, and to show that liquid supports relief the preexisting strain, have negligible doping effect and restore the uniformity of the properties throughout the graphene sheet. Such an effect originates from the molecular smoothness, structural adaptability and flexibility, lesser contamination and weaker intermolecular bonding of liquids compared to solid supports, independently of the chemical nature of the liquid. Moreover, water provides a platform to study and distinguish chemical defects from substrate-induced defects, in the particular case of hydrogenated graphene. Liquid supports, thus, are advantageous over solid supports for a range of applications, particularly for monitoring changes in the graphene structure upon chemical modification.

3.1. Introduction

Graphene is typically perceived as a two dimensional film with outstanding electrical and optical properties, but unstable mechanically and, therefore, necessitating a solid support.[1–3] The use of supporting substrates restored the lacking mechanical stability and prompted the development of the vast variety of graphene-based devices, such as field effect transistors,[4,5] transparent conducting electrodes,[6] gas and pressure sensors,[7,8] DNA-single molecule detections, to name a few.[9,10] Although being widely adapted for the fabrication of current graphene-based devices and technologies, solid substrates largely affect graphene due to doping and induced strain, and thus hinder the intrinsic properties of graphene.[11–19] The effect is even more prominent for CVD (chemical vapor deposition)-grown graphene samples, in which numerous inhomogeneities, inevitably caused by the growth and transfer processes, result in a wide variability of the band structure (and thus Raman signature), not only from sample to sample, but also from spot to spot within a single graphene sample.[13–24] This chapter studies graphene supported by liquids, namely graphene at liquid/air and liquid/liquid interfaces, with the benefit of providing molecularly defined boundaries, unlike solid/graphene/air interfaces.

Graphene caged between two immiscible liquids displays strikingly higher charge carrier mobilities as compared to graphene supported by solid substrates, presumably attributed to fewer contamination and the absence of scattering from the substrate.[25] However, the exact effect of liquids on the morphology and the properties of large sheets of CVD-graphene has not been ascertained yet. Although Raman spectroscopy has been recently successfully applied to characterize graphene flakes exfoliated in water,[26,27] in that case Raman spectrum is acquired as an average spectrum over all dispersed flakes and does not provide information about strain level and deviations in a single graphene flake. Moreover, no characterization of CVD graphene at liquid-liquid interfaces has been reported so far.

By studying the effect that liquid interfaces have on the properties of graphene, this chapter demonstrates that a liquid can be a standalone support for graphene. Remarkably, confocal Raman spectroscopy on graphene free-floating at an water/air and water/oil interfaces has shown that graphene supported by

liquid(s) undergoes very small to zero strain and doping effect, compared to "conventional" solid-supported or free-standing graphene, known to be always subjected to strain and doping.[11–19] Additionally, a statistical analysis of the graphene Raman peaks showed that also the variations of strain and doping values across the graphene sheet are significantly smaller when supported by liquids, owing to a more homogeneous and molecularly-defined graphene-liquid interface, as opposed to graphene-solid interface. Finally, the exceptional uniformity of the Raman signature of graphene in a liquid environment was used to characterize the changes in the properties of graphene upon hydrogenation and upon modifying the liquid environment.

3.2. Results and discussion

3.2.1. Raman spectroscopy of graphene at liquid interfaces

Graphene floats when placed on the surface of water due to the water surface tension. This property is routinely used during the transfer of CVD graphene from a catalyst substrate – the graphene/catalyst stack is placed on the surface of an aqueous solution of an etchant until the catalyst if fully dissolved and the graphene sheet remains free-floating at the water/air interface.[28,29] Similarly, the use of a biphasic mixture of water (or an aqueous etchant solution) and a non-polar liquid causes the graphene/catalyst stack to float in between the two immiscible phases, which yields graphene free-floating at the liquid/liquid interface once the catalyst is etched away.[25] In such biphasic design graphene is supported and protected by liquids on its both sides and, therefore, is less subjected to contamination and mechanical perturbations.[25,30] However, up to now, the only experimental insight into the graphene properties *in situ* at liquid/liquid and liquid/air interfaces has been the increase in charge carrier mobilities as compared to solid-supported graphene samples,[25] which indeed could be indicative of reduced contamination and strain.

This chapter presents a Raman study of a single layer graphene at water/air, water/1-octanol and water/cyclohexane interfaces; graphene on copper (as-grown), free-standing graphene (transferred onto quantifoil grids with the

interfacial caging method[25]) and graphene transferred onto Si/SiO$_2$ wafers (transferred with the interfacial caging method[25]). All graphene samples were grown according to the same growth protocol. The measurements were conducted at two excitation wavelengths, 457 nm and 532 nm respectively (as the 457 nm better suits Raman measurements of graphene on copper, and 532 nm those of graphene on Si/SiO$_2$), see Figure 3.1. Noteworthy, detecting just a single layer of graphene on water or at a water/liquid interface is very challenging if not impossible with a conventional Raman spectrometer, due to much larger quantities and very intensive Raman bands of the liquids. A confocal Raman spectrometer, on the other hand, can provide spatial resolution sufficient for focusing on the graphene sheet and recording a Raman spectrum where the bands of graphene and of the liquids have comparable intensities.

The two most intensive Raman bands of pristine graphene are the G band at ~1585 cm^{-1} and 2D band at ~2700 cm^{-1} (for 532 nm excitation wavelength, Figure 3.1a) or at ~2730 cm^{-1} (for 457 nm excitation wavelength, Figure 3.1b). The G band originates from a first-order one-phonon scattering process and the 2D band from a second-order two-phonon intervalley scattering process, and are both typical of all sp^2 carbon materials.[31] The frequencies, intensities and linewidths of the G and 2D bands of graphene are affected by the laser excitation energy (of the G band negligibly), number of graphene layers, strain and doping.[31,32] Presence of defects in graphene lattice (including rehybridization of sp^2 bonds due to chemical functionalization) breaks the symmetry and activates the D band at ~1350 cm^{-1}. The relative intensity of the D band with respect to the G band is commonly used to characterize the amount of defects and disorder in graphene materials.

Graphene Raman bands can be unambiguously distinguished from the Raman bands of the liquids (as seen from Figure 3.1 and Table A2.1 in Appendix 2). The only overlap occurs between the 2D band of graphene and one of the bands of 1-octanol at ~2730 cm^{-1} measured with 457 nm laser wavelength. But given that the 2D band of graphene is at least three times as intensive, the overlap does not hinder the determination of the 2D band position (Figure 3.1a, c). At an excitation wavelength of 532 nm, the two peaks are fully resolved as the 2D band is downshifted by ~30 cm^{-1} due to dispersion (Figure 3.1b, d).
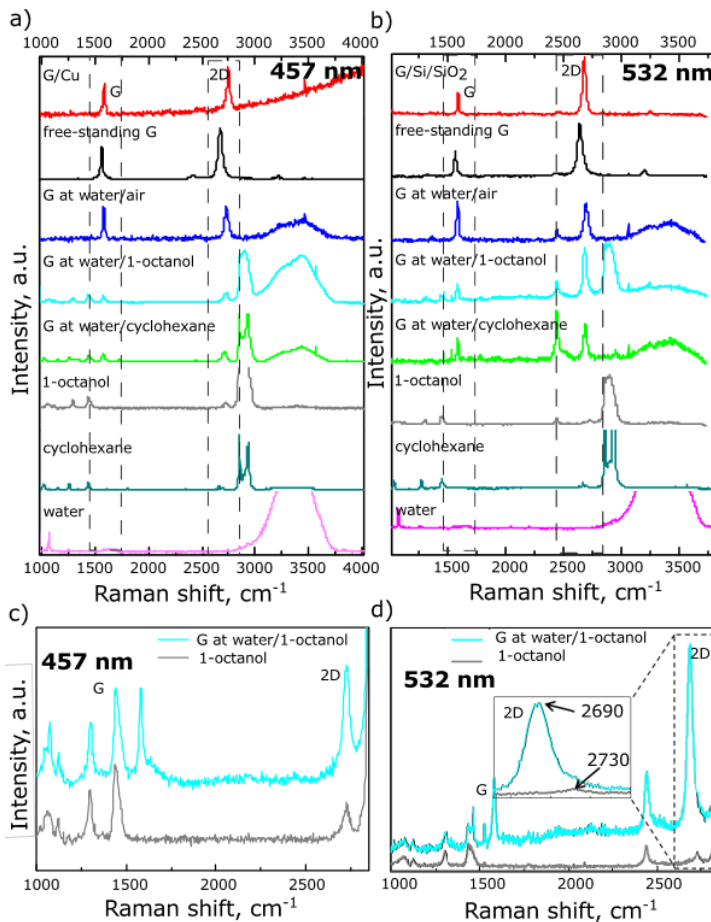
Figure 3.1. Raman spectra of graphene on different solid and liquid supports. a) Graphene-on-copper, free-standing graphene on a quantifoil grid, graphene at a water/air interface, graphene at a water/1-octanol interface, graphene at a water/cyclohexane interface, pure 1-octanol, pure cyclohexane, pure water. Laser excitation wavelength is 457 nm. b) Graphene on a Si/SiO$_2$ wafer, free-standing graphene on a quantifoil grid, graphene at a water/air interface, graphene at a water/1-octanol interface, graphene at a water/cyclohexane interface, pure 1-octanol, pure cyclohexane, pure water. Laser excitation wavelength is 532 nm. c) The Raman spectra of graphene at a water/1-octanol interface and of pure 1-octanol recorded at an excitation wavelength of 457 nm. The G and 2D peaks of graphene are distinguishable from the peaks of 1-octanol. d) The Raman spectra of graphene at water/1-octanol interface and pure 1-octanol recorded at 532 nm wavelength. The G and 2D peaks of graphene are distinguishable from the peaks of 1-octanol (see the inset).

Interestingly, by an in-depth Raman scanning of graphene at a liquid/liquid interface and profiling the intensities of the G and 2D modes of graphene the position of the interface can be determined (with a ~800 nm resolution limited by the instrument), while no information about the location of the interface can be obtained by profiling the peaks of the liquids (see Figures A2.1 and A2.2 in Appendix 2).

3.2.2. Graphene supported by water is strain- and doping-free

The detailed analysis of Raman peaks shifts provides information about strain and doping in the graphene lattice, and, therefore, about the effect of the substrate and environment on graphene intrinsic properties. Strain and doping induced by the substrate and by the environment are known to alter the frequencies of the G and 2D bands of graphene (w_G and w_{2D} respectively), and, in fact, can be quantified based on the shifts of the Raman bands.[31,32] Moreover, a correlative analysis of the G and 2D peaks frequencies allows for the disentanglement of the effects of strain and doping.[15,30] For that, the measured frequencies of G and 2D bands are plotted on a scatter plot with a non-orthogonal strain-doping framework (the so called correlation map, see Figure 3.2). Essentially, the black non-orthgonal axes titled as "hydrostatic strain", "n-doping" and "p-doping" in Figure 3.2 represent frequencies of purely strained (doping-free) and purely doped (strain-free) graphene (and are determined theoretically and experimentally[16]), and their intersection point represents unstrained and undoped graphene.[34] Projections of a given data point on the strain and doping axes provide the values of strain and doping[16,33,35] (differentiating between p- and n-doping, however, is not possible solely based on the Raman data, hence both types of doping are represented). The correlation maps at 457 and 532 nm wavelengths were recalculated based on a 2D mode dispersion of 100 cm^{-1}eV^{-1}[36].

Remarkably, the correlation analysis of G and 2D frequencies of graphene in Figure 3.2 displayed two critical distinctions of graphene supported by liquids from graphene supported by solid substrates and from free-standing graphene: very small absolute values and very small deviations of strain and doping induced by the liquids.

68

Generally, the substrate and environment always induce strain and doping in graphene. Achieving a fully strain- and doping-free graphene area requires meticulous fabrication of a free-standing sheet suspended in a very particular geometry (across a circular well).[16] In fact, the broadly scattered data points and wide frequency histograms in Figure 3.2 for graphene on copper, graphene on Si/SiO$_2$ and free-standing graphene indicate wide variations of strain and doping in these samples. Particularly, as seen from Figure 3.2a graphene on copper (the growth substrate) undergoes a wide range of strain values – from -0.8% (compressive strain) till 0.7% (tensile strain) with no evident dominating values (see wide frequency distribution histograms in Figure 3.2a). Importantly, such ununiformity of strain values occurs from spot to spot within a single graphene sheet, and is reproduced in all samples of graphene-on-copper (see Figure A2.3a in Appendix 2 for sample-to-sample variations). The wide variations of the strain level are typical for CVD graphene on copper and originate from the mismatch of the lattice parameters between graphene and copper and from the inhomogeneity of the surface of copper (differently oriented domains, grain boundaries, defects, steps in the case of unpolished polycrystalline copper).[17,20–23]

Similarly, free-standing graphene also exhibits very wide strain variations, ranging from -0.1% to 1% (Figure 3.2 and Figures A2.3b and A2.3c in Appendix 2), indicating that the free-standing configuration induces predominantly tensile strain. Strain is known to vary significantly from spot to spot in suspended graphene films depending on the position of the spot with respect to the center and the supported part.[17,37] Importantly, the measured strain values for free-standing CVD graphene are higher than those reported for an exfoliated free-standing graphene flake,[37] demonstrating that the CVD growth and possibly the transfer process induce the strain field that remains in graphene even when it is suspended, i.e. is in a potentially zero- or low-strain geometry.

Si/SiO$_2$ substrate is known to have a strain relaxation effect on graphene,[22] and in fact, graphene transferred onto a Si/SiO$_2$ wafer exhibits much narrower data scattering and strain variation from -0.3% to 0.2% (Figure 3.2b and Figure A2.3d in Appendix 2).
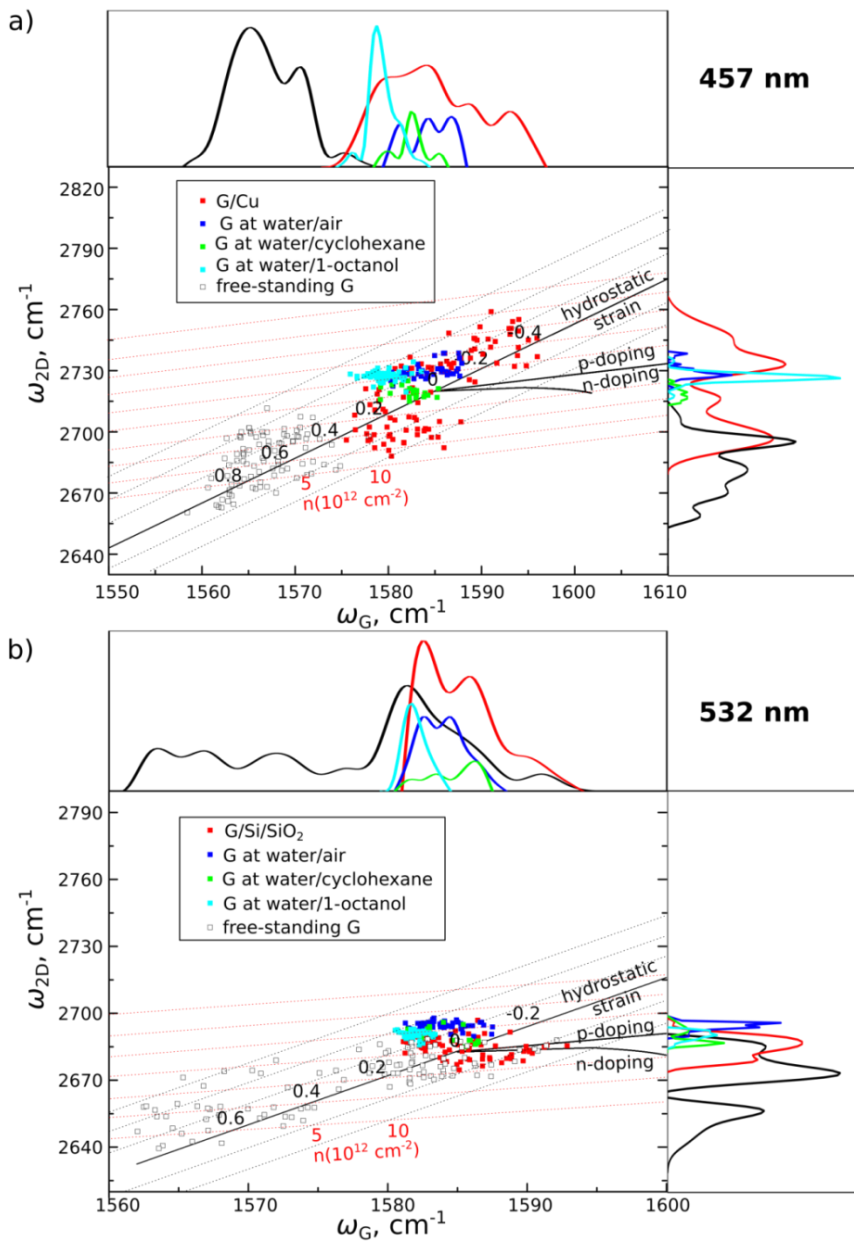
Figure 3.2. Correlation maps and statistical distributions of G and 2D Raman frequencies (w_G and w_{2D}) for graphene on different solid and liquid supports. a) Graphene on copper, graphene at water/air interface, graphene at water/cyclohexane interface, graphene at water/1-octanol interface and free-standing graphene on a quantifoil grid.

Black and red dash lines represent the strain and doping axes respectively. Laser excitation wavelength is 457 nm. b) Graphene on Si/SiO$_2$ wafer, graphene at water/air interface, graphene at water/cyclohexane interface, graphene at water/1-octanol interface, and free-standing graphene on a quantifoil grid. Black and red dash lines represent the strain and doping axes respectively. Laser excitation wavelength is 532 nm.

In contrast to the solid-supported and free-standing graphene, graphene floating at a water/air or a water/oil interfaces displays notably lower strain values and variations (Figure 3.2). Strain values of graphene at the water/air, water/cyclohexane and water/1-octanol cluster around zero with deviations within 0.1% (Figure 3.2).

In addition to lower strain, the correlation maps in Figure 3.2 also indicate lower and more uniform doping levels in the samples of graphene at liquid interfaces (compared to graphene on solid supports). Specifically, for all graphene samples at liquid interfaces the doping values deviate in the range of 2×10^{12} cm^{-2}- 3×10^{12} cm^{-2}, up to 10×10^{12} cm^{-2} for graphene on copper and free-standing graphene, and up to 8×10^{12} cm^{-2} for the graphene on Si/SiO$_2$ (Figure 3.2).

Remarkably, graphene on water shows similar level of doping and slightly lower fluctuations of strain compared to graphene supported by h-BN (Figure A2.5 in Appendix 2). H-BN is known as a solid substrate with the best conformity to graphene and lowest induced strain and doping, allowing for the highest charge carrier mobilities reported for graphene.[38,39] Important to note, however, that only CVD graphene on CVD h-BN (as a comparison to the CVD graphene in liquids) was studied in this work, while lower levels of strain and doping might be observed in mechanically exfoliated flakes of graphene on h-BN.

Figure 3.2 shows that the position of the Raman 2D band is a particularly evident distinction between the graphene supported by the liquids and graphene supported by solid substrates: the distribution histograms for all liquids are narrow with average values of ~2727 cm^{-1} (457 nm excitation wavelength, Figure 3.2a) and ~2690 cm^{-1} (532 nm excitation wavelength, Figure 3.2b). The G band, on the other hand, is less sensitive to strain,[40,41] and therefore, is not indicative of strain-induced changes in graphene properties, although narrower distributions of the G band positions in Figure 3.2 do point at better uniformity of graphene-liquid interfaces as opposed to graphene-solid interfaces.

Additionally to the band frequencies, the full widths at half-maximum (FWHM) of the G and 2D bands (denoted here Γ_G and Γ_{2D} respectively) can also be used for monitoring strain and doping in graphene (Figure 3.3). A narrower G band corresponds to a larger charge doping,[42] and a broadening of the 2D band suggests a nonuniform anisotropic character of strain.[20,32,43] Although graphene supported by liquids displays more uniform strain fields than graphene on solids (Figure 3.2), the 2D bandwidths of graphene on liquids are similar to those of graphene on solids (Figure 3.3). Such broadening of the 2D band of graphene on liquids is likely to be caused by instrumental factors: Raman spectra of graphene floating in liquids typically have higher noise levels (due to vibrations on the liquid surface causing the graphene to fluctuate from the focal plane of the microscope) than those of graphene on solid substrates, leading to less accurate determination of peak widths. The positions of peaks maximums, on the other hand, are not affected by increased noise level and can be determined accurately.

Overall, replacing solid supports with liquid(s) results in an articulate relaxation of strain and reduction of doping level in graphene sheet. Additionally, the spot-to-spot deviations of strain and doping within the graphene sheet are significantly smaller for liquid-supported graphene, indicating more uniform properties of the graphene surface.

Importantly, the observed effects are stable in time, and the Raman signature and statistical distributions of the strain and doping values in graphene-on-water remained unchanged even after floating on the surface of water for eight days (Figure A2.6 in Appendix 2).
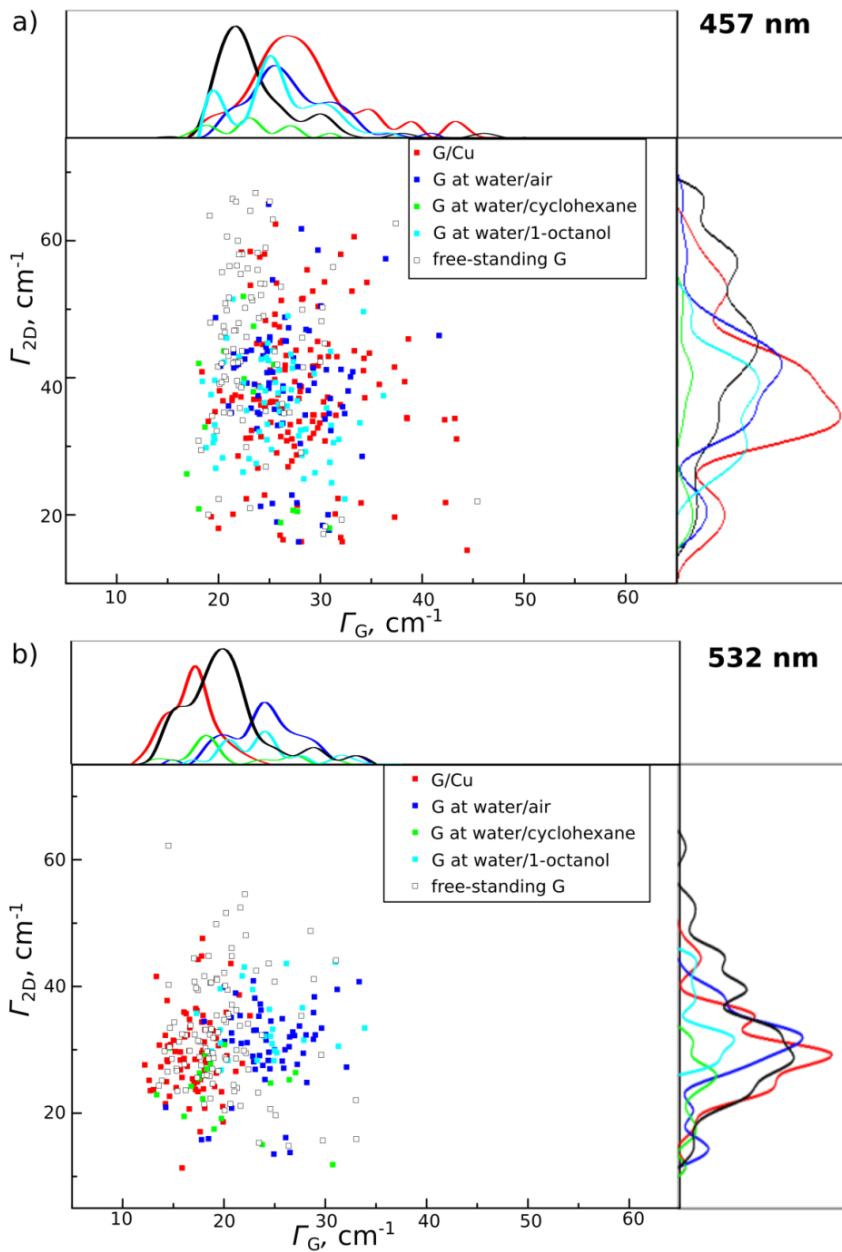
Figure 3.3. Correlation maps and statistical distributions of G and 2D Raman full widths at half maximum (FWHM or Γ_G and Γ_{2D}) for graphene on different solid and liquid supports. a) Graphene on copper, graphene at water/air interface, graphene at water/cyclohexane interface, graphene at water/1-octanol interface and free-standing

graphene on a quantifoil grid. Laser excitation wavelength is 457 nm. b) Graphene on Si/SiO$_2$ wafer, graphene at water/air interface, graphene at water/cyclohexane interface, graphene at water/1-octanol interface, and free-standing graphene on a quantifoil grid. Laser excitation wavelength is 532 nm.

3.2.3. Effects of different liquid environment on strain and doping in floating graphene

Next, the effects of different liquid interfaces on strain and doping levels of graphene were examined, based on the correlation map of G and 2D bands positions (Figure 3.4). Four different interfaces namely water/air, water/cyclohexane, water/1-octanol and deuterated water/air were studied. Interestingly, the data points for all interfaces are tightly clustered with small deviations from the point of zero strain and doping (within 0.1-0.2% for strain and 2×10^{12} - 3×10^{12} cm^{-2} for doping, see Figure 3.4a and b).

As seen from the scattering of the data points in Figure 3.4a and b, graphene at water/1-octanol interface seems to undergo slightly lower and more uniform strain and doping than at water/cyclohexane interface, which can be attributed to a lower polarity gradient and stronger association (between the liquids) of the water/1-octanol interface.[44] Interestingly, compared to the graphene at the water/1-octanol and water/cyclohexane interfaces, graphene at water/air and deuterated water/air interfaces exhibit more uniform strain distributions, but also are slightly more doped (Figure 3.4a, b).
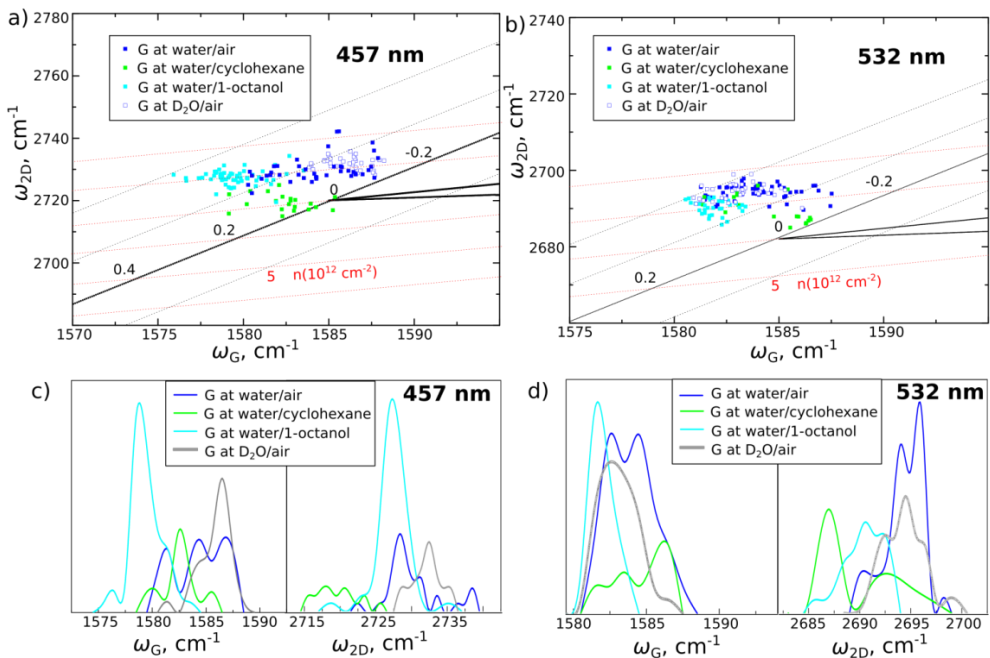
Figure 3.4. Effects of different liquid environment on strain and doping in floating graphene a) Correlation map of G and 2D band frequencies (w_G and w_{2D}) for graphene at the water/air interface, graphene at the water/cyclohexane interface, graphene at the water/1-octanol interface and graphene at the deuterated water/air interface. Laser excitation wavelength is 457 nm. b) Correlation map of G and 2D Raman frequencies (w_G and w_{2D}) for graphene at the water/air interface, graphene at the water/cyclohexane interface, graphene at the water/1-octanol interface and graphene at the deuterated water/air interface. Laser excitation wavelength is 532 nm. c) Statistical distributions of G and 2D Raman frequencies (w_G and w_{2D}) for graphene at water/air interface, graphene at water/cyclohexane interface, graphene at water/1-octanol interface and graphene at deuterated water/air interface. Laser excitation wavelength is 457 nm. d) Statistical distributions of G and 2D Raman frequencies (w_G and w_{2D}) for graphene at water/air interface, graphene at water/cyclohexane interface, graphene at water/1-octanol interface and graphene at deuterated water/air interface. Laser excitation wavelength is 532 nm.

The observed differences in strain and doping levels of graphene at different liquid interfaces are, therefore, insignificant, especially in contrast with their drastic difference from the strain and doping levels in graphene on solid

substrates demonstrated above. Remarkably, dissimilarities in the properties of the liquid interfaces, such as interfacial tensions, polarity gradients and intermolecular bonding did not have significantly different effect on the Raman signature of graphene.

Importantly, liquid/graphene/air and liquid/graphene/liquid interfaces are molecularly smooth, which was confirmed at least for the case of water/graphene interface by MD simulations (Figure A2.7 in Appendix 2), especially when compared to graphene in vacuum. This implies that the molecular smoothness together with the structural adaptability of liquid interfaces are likely to be the causes of the strain relaxation effect, irrespective of the chemical and physical properties of the liquids.

3.2.4. Raman spectroscopy of graphene on liquid supports to characterize functionalization of graphene

Finally, liquid supports were utilized to characterize the properties of graphene upon functionalization, specifically on the example of hydrogenation of graphene. Hydrogenated graphene (h-G) is typically characterized by the position (w_D) and relative intensity (the ratio between the intensities of the D and the G bands, or the I_D/I_G ratio) of the Raman D band arising from the formation of C-H bonds and rehybridization of the graphene lattice from sp^2 to sp^3.[45,46] Two types of samples with different hydrogenation degrees were prepared using a hydrogen plasma on graphene grown on copper (see Methods In Appendix 2 for details) – with plasma treatment duration of respectively 10 s and 60 s.[47] Raman spectra were recorded for a pristine graphene on copper and on water (the same graphene sheet before and after etching the copper and replacing the etchant with pure water) and for hydrogenated graphene samples on copper and water (same samples of hydrogenated graphene before and after etching the copper and replacing the etchant with pure water), Figure 3.5.

First, for the samples that underwent 10 s of hydrogenation, h-G floating on water have much narrower distributions of the D peak position w_D compared to that of h-G on copper (1368±1 cm^{-1} for h-G/water versus 1376±5 cm^{-1} for h-G/Cu, see Figure 3.5a). Similarly, the distribution of the D peak width Γ_D is also narrower

for h-G on water as opposed to h-G on copper (Figure A2.4a in Appendix 2). The narrower distribution of w_D values in the case of h-G/water (Figure 3.5a) suggests the dominance of only one type of defects (hydrogenation-caused sp^3 carbon atoms), while in the case of h-G/Cu the multimodal distribution of w_D must be caused by a different types of defects (sp^3 carbon atoms and other defects not related to hydrogenation) or doping effect.[48,49] The samples of h-G/Cu and h-G/water are, however, essentially the same sheet of graphene tested before and after copper etching, and, in principle, should have identical types and amounts of defects. The main differences between the samples (accounting for the difference in D peaks) are the different levels of strain and doping induced by copper and water. In fact, although strain *per se* does not generate a D peak in graphene, the strain fields in graphene induced by copper can activate defects such as interstitials and vacancies along the grain boundaries of graphene,[50] resulting in the shift and broadening of the D peak. This does not take place in the samples of h-G/water, because of lower strain induced by water (Figure 3.5c). Additionally, due to inhomogeneous strain fields in h-graphene on copper, there is a variation of C-H bond lenghs across the h-graphene sheet, also resulting in the variation of the phonon frequencies (i.e. D peak positions).

In addition to strain-activated defects, doping is also known to cause shift in the D mode frequency and alter the D mode intensity.[48,49] As shown in Figure 3.2a, copper induces significantly higher and more inhomogeneous doping levels in graphene compared to water. As a result, the inhomogeneous doping (i.e. different doping values across the sample) in the case of copper causes a wider variation in the D peak frequencies and intensities.

Using water as a substrate, therefore, allows extracting the effect of hydrogenation from substrate-activated defects. Furthermore, not only the w_D, but also the I_D/I_G ratio displays a lower variability across the h-G sheet when supported by water as opposed to copper (Figure 3.5b). Since in the case of h-G/water the D peak originates solely from hydrogenation, the I_D/I_G histogram of h-G/water is a better estimate of hydrogenation degree than that of h-G/Cu. Interestingly, the I_D/I_G histogram of h-G/Cu would mistakenly indicate a less uniform (compared to h-G/water) hydrogenation of the graphene sheet (Figure 3.5b). Given that the graphene sheets in h-G/water and h-G/Cu have identical degree and distribution of hydrogenation, the wider I_D/I_G histogram of h-G/Cu

thus proves the contribution of substrate-activated defects and doping in the intensity of the D peak.

Finally, variations in strain and doping levels can be assessed based on the correlation map of G and 2D bands in Figure 3.5c. h-G/water displays slightly lower variations (within 10^{13} cm^{-2}) of doping levels than h-G/Cu (within 15×10^{12} cm^{-2}), which confirms that doping can be one of the reasons for the inhomogeneity of the D band position and intensity in the case of h-G/Cu. Similarly to pristine graphene, hydrogenated graphene is also subjected to greater and less uniform strain on copper, varying from -0.6 % to 0.1 %, than it is on water, where the strain varies from -0.2 % to 0 % (Figure 3.5c). Interestingly, graphene became slightly more doped after the hydrogenation, with the doping values varying from 2×10^{12} cm^{-2} to 12×10^{12} cm^{-2} for h-G/water and from 0 to 5×10^{12} cm^{-2} for the G/water, as seen from the correlation map for h-G/water and G/water (Figure 3.5c). Strain levels, on the other hand, remain low and unaffected by hydrogenation and vary between 0 and 0.2 % both for G/water and h-G/water (Figure 3.5c). Measurements on copper, in contrast, do not allow differentiating between G/Cu and h-G/Cu due to the wide variations of strain (Figure 3.5c).

For 60 s hydrogenation, results are similar to the 10 s hydrogenation (Figure 3.5d-f). The narrow distributions and the same mean values of w_D and Γ_D in the both cases (Figure 3.5d and Figure A2.4b in Appendix 2) demonstrate that the D peak of h-G/water reflects the hydrogenation effect (and not other defects) and is, therefore, a better indication of hydrogenation than the D peak of h-G/Cu. Interestingly, comparison between the I_D/I_G distributions of h-G/water in Figure 3.5b and 3.5e demonstrates that longer plasma exposure results in higher and less uniform hydrogenation of the graphene, which is in agreement with previous studies.[51,52] Even more pronouncedly than in the case of 10s hydrogenation (Figure 3.5c), hydrogenation for 60 s results in higher doping values than in pristine graphene, from 0-5$\times 10^{12}$ cm^{-2} for G/water to 5-15$\times 10^{12}$ cm^{-2} for h-G/water (Figure 3.5f). Increased doping levels in hydrogenated graphene compared to pristine graphene were also observed previously[45,53] and are linked to the difference in the work functions between graphene and the substrate.[54] The work function of graphene[54,55] is close to that of water,[56] which results in insignificant charge carrier transfer between graphene and the substrate, and, therefore, low

doping levels in G/water observed in our work. Due to rehybridization of carbon atoms and formation of C-H bonds, hydrogenation alters the work function of graphene,[57–59] increasing the difference with the work function of water and, therefore, facilitating doping of h-G.

Like in the case of 10 s hydrogenation, the strain levels did not change upon 60 s hydrogenation and are close to 0 with the deviations of 0.1 % for both G/water and h-G/water (Figure 3.5f).

By contrast, no conclusive evaluation of the hydrogenation effect can be made based on the data from h-G/Cu due to the higher variation in doping values ($\pm 10^{13}$ cm^{-2} versus $\pm 5 \times 10^{12}$ cm^{-2} for h-G/water) and possibly the presence of strain-activated defects (wide distribution histogram of w_D, Figure 3.5d) and their different contribution to the intensity of the D band (Figure 3.5e).[32] Large variations of strain in h-G/Cu (-0.2 %-0.6 %) and G/Cu (-0.3 %-0.5 %), however, result in overlapping and thus non-distinguishable data on the correlation maps of G and 2D bands for the pristine and hydrogenated graphene supported by copper (Figure 3.5f).
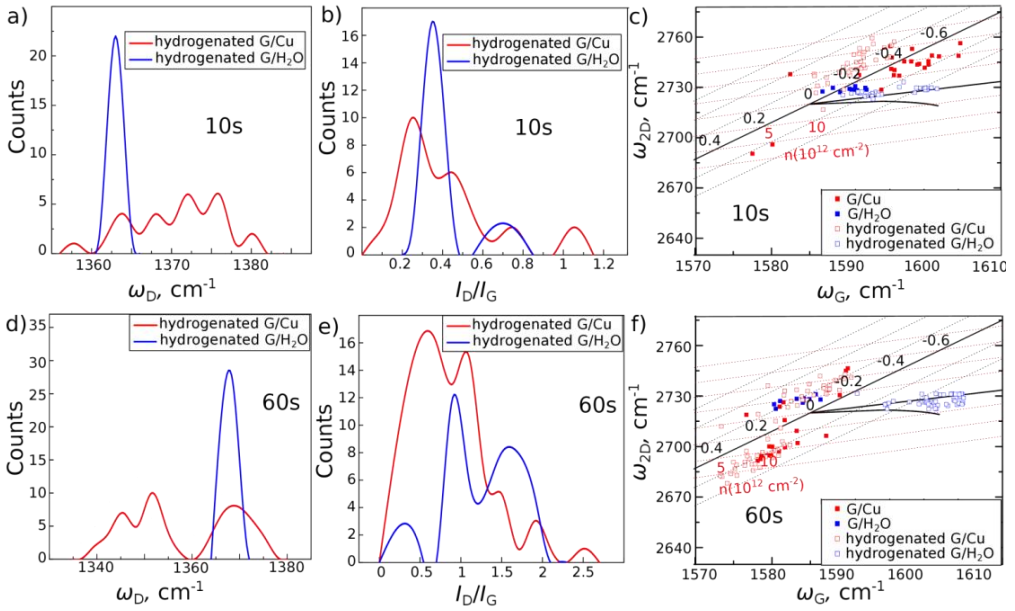
Figure 3.5. Raman analysis of hydrogenated graphene (h-G). a) Statistical distributions of D peak frequencies (w_D) of h-G on copper and water. Hydrogenation time was 10 s. b) Statistical distributions of I_D/I_G ratios of hydrogenated graphene (h-G) on copper and on water after etching the copper. Hydrogenation time was 10 s. c) Correlation map of G and 2D peaks frequencies of non-treated graphene on copper, non-treated graphene on water, h-G on copper and h-G on water. Hydrogenation time was 10 s. d) Statistical distributions of D peak frequencies (w_D) of h-G on copper and water. Hydrogenation time was 60 s. e) Statistical distributions of I_D/I_G ratios of hydrogenated graphene (h-G) on copper and on water after etching the copper. Hydrogenation time was 60 s. f) Correlation map of G and 2D peaks frequencies of non-treated graphene on copper, non-treated graphene on water, h-G on copper and h-G on water. Hydrogenation time was 60 s.

Ultimately, using water as a substrate minimizes the impact of the substrate not only on the G and 2D bands, directly responsive to strain, but also on the D band activated by defects in the graphene structure. Unlike hydrogenated graphene on copper, the D band of hydrogenated graphene on water originates solely from the hydrogenation effect, which allows accurately assessing the degree and

80

uniformity of hydrogenation and tracking the effect of hydrogenation on the strain and doping levels in graphene.

3.3. Conclusions

In a liquid attractive forces between the molecules are weaker than in a solid, allowing the molecules to move.[60,61] Continuous movement of molecules allows the formation of a homogeneous, energy-minimized, self-healing surface free of kinetic traps (and consequently, defects), which adapts to and takes the shape of the surface the liquid is in contact with, i.e. graphene in our case.[60,61] Homogeneity, molecular smoothness, structural adaptability of liquid interfaces are universal properties of all liquids, independently of their chemical nature.[60–62] Remarkably, various liquid interfaces relax and unify strain in graphene down to similar values, indicating that the structural, rather than chemical, properties of liquids are responsible for the strain relaxation effect.

In summary, graphene floating directly on a liquid or even buried in between two liquids was studied by Raman spectroscopy. All three major Raman bands of graphene – the D, G and 2D band remain unaffected by liquid substrates. Using liquids to support graphene, thus, can be beneficial over solid substrates whenever the properties of graphene need to be accurately monitored. Here the advantages of a water support were showcased through the example of hydrogenation of graphene, but can, in principle be applied for studying other effects on graphene structure.

3.4. References

1.   Lau, C. N., Bao, W. & Velasco, J. Properties of suspended graphene membranes. *Mater. Today* **15,** 238–245 (2012).

2.   Zandiatashbar, A. *et al.* Effect of defects on the intrinsic strength and stiffness of graphene. *Nat. Commun.* **5,** 3186 (2014).

3.   Zhang, P. *et al.* Fracture toughness of graphene. *Nat. Commun.* **5,** 3782 (2014).

4.   K. S. Novoselov, S. V. Morozov, D. Jiang, Y. Zhang, S. V. Dubonos, I. V. Grigorieva, A. A. Firsov, A. K. G. Electric field effect in atomically thin carbon films. *Science* **306,** 666–669 (2004).

5.   Lemme, M. C., Echtermeyer, T. J., Baus, M. & Kurz, H. A Graphene field-effect device. *IEEE Electron Device Lett.* **28,** 282–284 (2007).

6.   Matyba, P., Yamaguchi, H., Eda, G., Chhowalla, M., Edman, L. y Robinson, N. D. Graphene and mobile ions: the key to all plastic, solution processed light emitting devices. *ACS Nano* **4,** 637–642 (2010).

7.   Schedin, F. *et al.* Detection of individual gas molecules adsorbed on graphene. *Nat. Mater.* **6,** 652–655 (2007).

8.   Xu, Y. *et al.* In-plane and tunneling pressure sensors based on graphene/hexagonal boron nitride heterostructures. *Appl. Phys. Lett.* **99,** 1–4 (2011).

9.   Heerema, S. J. & Dekker, C. Graphene nanodevices for DNA sequencing. *Nat. Nanotechnol.* **11,** 127–136 (2016).

10. Arjmandi-Tash, H., Belyaeva, L. A. & Schneider, G. F. Single molecule detection with graphene and other two-dimensional materials: nanopores and beyond. *Chem. Soc. Rev.* **45,** 476–493 (2016).

11. Guinea, F., Katsnelson, M. I. & Geim, A. K. Energy gaps and a zero-field quantum Hall effect in graphene by strain engineering. *Nat. Phys.* **6,** 30–33 (2009).

12. Pereira, V. M. & Castro Neto, A. H. Strain engineering of graphene's electronic structure. *Phys. Rev. Lett.* **103,** 46801 (2009).

13. Bao, W. *et al.* Controlled ripple texturing of suspended graphene and ultrathin graphite membranes. *Nat. Nanotechnol.* **4,** 562–566 (2009).

14. Wang, Y. Y. *et al.* Raman studies of monolayer graphene: the substrate effect. *J. Phys. Chem. C* **112,** 10637–10640 (2008).

15. Hu, Z., Prasad Sinha, D., Lee, J. U. & Liehr, M. Substrate dielectric effects on graphene field effect transistors. *J. Appl. Phys.* **115,** (2014).

16. Lee, J. E., Ahn, G., Shim, J., Lee, Y. S. & Ryu, S. Optical separation of mechanical strain from charge doping in graphene. *Nat. Commun.* **3,** 1024 (2012).

17. Bendiab, N. *et al.* Unravelling external perturbation effects on the optical phonon response of graphene. *J. Raman Spectrosc.* **49,** 130–145 (2018).

18. Neumann, C. *et al.* Raman spectroscopy as probe of nanometre-scale strain variations in graphene. *Nat. Commun.* **6,** 8429 (2015).

19. Lee, Y. R., Huang, J. X., Lin, J. C. & Lee, J. R. Study of the substrate-induced strain of as-grown graphene on Cu(100) using temperature-dependent Raman spectroscopy: estimating the mode Grüneisen parameter with temperature. *J. Phys. Chem. C* **121,** 27427–27436 (2017).

20. He, R. *et al.* Large physisorption strain in chemical vapor deposition of graphene on copper substrates. *Nano Lett.* **12,** 2408–2413 (2012).

21. Yu, V., Whiteway, E., Maassen, J. & Hilke, M. Raman spectroscopy of the internal strain of a graphene layer grown on copper tuned by chemical vapor deposition. *Phys. Rev. B - Condens. Matter Mater. Phys.* **84,** 1–5 (2011).

22. Troppenz, G. V., Gluba, M. A., Kraft, M., Rappich, J. & Nickel, N. H. Strain relaxation in graphene grown by chemical vapor deposition. *J. Appl. Phys.* **114,** (2013).

23. Zhang, Y. *et al.* Defect-like structures of graphene on copper foils for strain relief investigated by high-resolution scanning tunneling microscopy. *ACS Nano* **5,** 4014–4022 (2011).

24. Yoon, D., Son, Y.-W. & Cheong, H. Negative thermal expansion coefficient of graphene measured by Raman spectroscopy. *Nano Lett.* **11,** 3227–3231 (2011).

25. Belyaeva, L. A., Fu, W., Arjmandi-Tash, H. & Schneider, G. F. Molecular caging of graphene with cyclohexane: transfer and electrical transport. *ACS Cent. Sci.* **2,** 904–909 (2016).

26. Mary, R. *et al.* 1.5 GHz picosecond pulse generation from a monolithic waveguide laser with a graphene-film saturable output coupler. *Opt. Express* **21,** 7943–7950 (2013).

27. Bepete, G., Pénicaud, A., Drummond, C. & Anglaret, E. Raman signatures of single layer graphene dispersed in degassed water, ''Eau de Graphene''. *J. Phys. Chem. C* **120,** 28204–28214 (2016).

28. Reina, A. *et al.* Transferring and identification of single- and few-layer graphene on arbitrary substrates. *J. Phys. Chem. C* **112,** 17741–17744 (2008).

29. Li, X. *et al.* Large-area synthesis of high-quality and uniform graphene films on copper foils. *Science* **324,** 1312–1314 (2009).

30. Zhang, G. *et al.* Versatile polymer-free graphene transfer method and applications. *ACS Appl. Mater. Interfaces* **8,** 8008–8016 (2016).

31. Malard, L. M., Pimenta, M. A., Dresselhaus, G. & Dresselhaus, M. S. Raman spectroscopy in graphene. *Phys. Rep.* **473,** 51–87 (2009).

32. Ferrari, A. C. & Basko, D. M. Raman spectroscopy as a versatile tool for studying the properties of graphene. *Nat. Nanotechnol.* **8,** 235–246 (2013).

33. Mueller, N. S. *et al.* Evaluating arbitrary strain configurations and doping in graphene with Raman spectroscopy. *2D Mater.* **5,** 15016 (2018).

34. Frank, O. *et al.* Phonon and structural changes in deformed bernal stacked bilayer graphene. *Nano Lett.* **12,** 687–693 (2012).

35. Froehlicher, G. & Berciaud, S. Raman spectroscopy of electrochemically gated graphene transistors: Geometrical capacitance, electron-phonon, electron-electron, and electron-defect scattering. *Phys. Rev. B* **91,** 205413 (2015).

36. Costa, S. D. *et al.* Resonant Raman spectroscopy of graphene grown on copper substrates. *Solid State Commun.* **152,** 1317–1320 (2012).

37. Metten, D., Federspiel, F., Romeo, M. & Berciaud, S. Probing built-in strain in freestanding graphene monolayers by raman spectroscopy. *Phys. Status Solidi Basic Res.* **250,** 2681–2686 (2013).

38. Wang, L. *et al.* One-dimensional electrical contact to a two-dimensional material. *Science* **342,** 614–617 (2013).

39. Banszerus, L. *et al.* Ultrahigh-mobility graphene devices from chemical vapor deposition on reusable copper. *Sci. Adv.* **1,** e1500222 (2015).

40. Teague, M. L. *et al.* Evidence for strain-induced local conductance modulations in single-layer graphene on SiO 2. *Nano Lett.* **9,** 2542–2546 (2009).

41. Huang, M., Yan, H., Heinz, T. F. & Hone, J. Probing strain-induced electronic structure change in graphene by Raman spectroscopy. *Nano Lett.* **10,** 4074–4079 (2010).

42. Yan, J., Zhang, Y., Kim, P. & Pinczuk, A. Electric field effect tuning of electron-phonon coupling in graphene. *Phys. Rev. Lett.* **98,** 166802 (2007).

43. Yoon, D., Son, Y.-W. & Cheong, H. Strain-dependent splitting of the double-resonance Raman scattering band in graphene. *Phys. Rev. Lett.* **106,** 155502 (2011).

44. Steel, W. H. & Walker, R. A. Measuring dipolar width across liquid-liquid interfaces with 'molecular rulers'. *Nature* **424,** 296–299 (2003).

45. Elias, D. C. *et al.* Control of graphene's properties by reversible hydrogenation: evidence for graphane. *Science* **323,** 610–613 (2009).

46. Cançado, L. G. *et al.* Quantifying defects in graphene via Raman spectroscopy at different excitation energies. *Nano Lett.* **11,** 3190–3196 (2011).

47. Jiang, L., Fu, W., Birdja, Y. Y., Koper, M. T. M. & Schneider, G. F. Quantum and electrochemical interplays in hydrogenated graphene. *Nat. Commun.* **9,** 793 (2018).

48. Liu, J. *et al.* The dependence of graphene Raman D-band on carrier density. *Nano Lett.* **13,** 6170–6175 (2013).

49. Bruna, M. *et al.* Doping dependence of the Raman spectrum of defected

graphene. *ACS Nano* **8,** 7432–7441 (2014).

50. Wang, B., Puzyrev, Y. & Pantelides, S. T. Strain enhanced defect reactivity at grain boundaries in polycrystalline graphene. *Carbon N. Y.* **49,** 3983–3988 (2011).

51. Whitener, K. E., Robinson, J. T. & Sheehan, P. E. Protection from below: stabilizing hydrogenated graphene using graphene underlayers. *Langmuir* **33,** 13749–13756 (2017).

52. Bangert, U., Pan, C. T., Nair, R. R. & Gass, M. H. Structure of hydrogen-dosed graphene deduced from low electron energy loss characteristics and density functional calculations. *Appl. Phys. Lett.* **97,** 253118 (2010).

53. Matis, B. R. *et al.* Surface doping and band gap tunability in hydrogenated graphene. *ACS Nano* **6,** 17–22 (2012).

54. Niesner, D. & Fauster, T. Image-potential states and work function of graphene. *J. Phys. Condens. Matter* **26,** 393001 (2014).

55. Yu, Y.-J. *et al.* Tuning the graphene work function by electric field effect. *Nano Lett.* **9,** 3430–3434 (2009).

56. Olivieri, G., Goel, A., Kleibert, A., Cvetko, D. & Brown, M. A. Quantitative ionization energies and work functions of aqueous solutions. *Phys. Chem. Chem. Phys.* **18,** 29506–29515 (2016).

57. Peng, X., Tang, F. & Copple, A. Engineering the work function of armchair graphene nanoribbons using strain and functional species: a first principles study. *J. Phys. Condens. Matter* **24,** 75501 (2012).

58. Leenaerts, O., Peelaers, H., Hernández-Nieves, A. D., Partoens, B. & Peeters, F. M. First-principles investigation of graphene fluoride and graphane. *Phys. Rev. B* **82,** 195436 (2010).

59. Wang, M., Zhou, Y., Kong Hark, S. & Zhu, X. A saw-tooth scaling of work function in hydrogenated graphene. *Preprint at http://arXiv.org/1707.07784* (2017).

60. Hansen, J.-P. & R. McDonald, I. Theory of simple liquids: with applications to soft matter: fourth edition. *Elsevier* (2013).

61. Fawcett, W. R. Liquids, solutions, and interfaces : from classical

macroscopic descriptions to modern microscopic details. *Oxford Univ. Press* (2004).

62. Ninham, B. & Lo Nostro, P. Molecular forces and self- assembly: in colloid, nano sciences and biology. *Phys. Today* **64,** (2010).